*Environmental Engineering and Management Journal*

*May 2020, Vol.19, No. 5, 849-860*
*http://www.eemj.icpm.tuiasi.ro/; http://www.eemj.eu*

*"Gheorghe Asachi" Technical University of Iasi, Romania*

# SYNERGISTIC EFFECT OF FUEL AGENTS AND MASS RATIO FOR MORPHO-STRUCTURAL OPTIMIZATION OF MAGNETIC CLAY-BASED NANOCOMPOSITES WITH HIGH ADSORPTION CAPACITY

**Stefana Cojocaru[1], Adrian Iulian Borhan[2,3]*, Alexandra Raluca Iordan[2]*, Mircea Nicolae Palamaru[2], Simona Cucu-Man[2], Vasile Hulea[4], Nicoleta Melniciuc-Puica[5], Ioan Dumitru[6], Tiberiu Roman[2,7], Iuliana Gabriela Breaban[1]**

*[1]"Alexandru Ioan Cuza" University of Iasi, Faculty of Geography and Geology,20A Carol I Blvd., 700505, Iasi, Romania*
*[2]"Alexandru Ioan Cuza" University of Iasi, Faculty of Chemistry,11Carol I Blvd., 700506, Iasi, Romania*
*[3]National Institute of Research and Development for Technical Physics,47 Mangeron Blvd., Iasi 700050, Romania*
*[4]"Charles Gerhardt" Institute, Montpellier, UMR 5253, CNRS-UM2-ENSCM-UM1, Matériaux Avancés pour la Catalyse et la Santé, 8 rue de l'Ecole Normale,34296 Montpellier Cedex 5, France*
*[5]"Alexandru Ioan Cuza" University of Iasi, Faculty of Orthodox Theology,9 Closca str., 700065, Iaşi, Romania*
*[6]"Alexandru Ioan Cuza" University of Iasi, Faculty of Physics, 11Carol I Blvd., 700506, Iasi, Romania*
*[7]"Gheorghe Asachi" Technical University of Iasi, Faculty of Materials Science and Engineering, 61A Mangeron Blvd., 700050 Iasi, Romania*

## Abstract

The study is focused on creating magnetic mesoporous materials through the insertion of a nickel ferrite into the structure of kaolin-type clay. Sol-gel auto-combustion method was employed to synthesize the materials, using glycine and tartaric acid as chelating/combustion agents. This is the first study on the combined effect of different fuel agents and of clay-to-ferrite molar ratio on the structural, textural, magnetic and adsorptive properties of nanocomposites. The value of the average pore size, registered in a range of 6.01 and 12.9 nm, indicates the dependence on both molar ratio and fuel agent. The textural properties of the materials, corroborated with those obtained from XRD, SEM and TEM and VSM, suggest that magnetic nanocomposites can be successfully used as adsorbents in the removal of harmful organics. The obtained nanocomposites show excellent adsorption, with up to 98% BB41 dye removal, and a facile recuperation, due to their magnetic properties. The maximum adsorption capacity of dye, of 752.2 mg/g, was obtained for C3Ni_act350, in the presence of $H_2O_2$ in solution. More than that, the adsorption capacity of magnetic composites increased with increasing the $NiFe_2O_4$ content.

*Key words:* adsorption, composite nanomaterials, dye, kaolin, magnetic separation, Ni ferrite

*Received: July, 2019; Revised final: November, 2019; Accepted: December, 2019; Published in final edited form: May, 2020*

## 1. Introduction

The use of natural materials in environmental remediation processes is desirable, due to their low cost and safety. Among the materials which have been used to improve water quality, mention should be made of clays, due to their good adsorptive capabilities as well as to the negative electrical charge of their surface, meaning they can attract and hold various ions (Oliveira et al., 2003; Peng et al., 2016).

Recent advances have been made towards improving their innate properties by their functionalization (Saravanan et al., 2020; Sivashankar et al., 2014). When using clays as adsorbents for organic pollutants, a difficulty encountered is their removal from the effluent. A solution is to functionalize them, for creating a magnetic composite,

* Author to whom all correspondence should be addressed: e-mail: alexandra.iordan@uaic.ro; adi.borhan@yahoo.com

which can be easily extracted using an exterior magnetic field (Bourlinos et al., 2002; Mehta et al., 2015; Safarik and Safarikova, 2010; Safarik et al., 2012; Zhou and Keeling, 2013). One of the most suitable materials to be inserted into the structure of clays are ferrites, nano-sized compounds with the general formula $MFe_2O_4$, recognized for their good magnetic properties (Shanmugavel et al., 2015; Sharma et al., 2018). Functionalized magnetic nanoparticles have recently been examined as a promising solution for adsorption of toxic dye pollutants (Ai et al., 2011; Hao et al., 2018; Hashem, 2012; Hashemian, 2011; Joshi et al., 2019; Kanwal et al., 2017; Makarchuk et al., 2016; Mohagheghian et al., 2017; Qu et al., 2013; Tamjidi et al., 2019; Teng et al., 2019; Wu et al., 2011).

The present study is the first of the investigations aimed at investigating the combined effect of different chelating/combustion agents (glycine and tartaric acid) and of the mass ratio of clay-to-ferrite (3:1, 4:1, 5:1) on the structural, textural, magnetic and adsorptive properties of magnetic composites consisting of a kaolin clay and nickel ferrite ($NiFe_2O_4$), by the sol-gel auto-combustion method. Nickel ferrite, a soft magnetic material with an inverted cubic spinel structure, was preferred for its magnetic behavior and chemical stability even at low heating temperature (Kaur et al., 2015; Shanmugavel et al., 2015).

Hence, nickel ferrite magnetizes the clay for its further extraction from the solution after the adsorption processes. This aspect is extremely important from the viewpoint of possible industrial scale use, as the composites can be recovered from the remediated water and regenerated for a new use. Optimization of the microstructure and morphologies of composites by using various fuel agents and mass ratio agents was a challenge for controlling their magnetic and adsorptive properties.

The synergetic effect of the adsorptive and catalytic properties (by using an oxidizing agent, $H_2O_2$) of the nanocomposite materials created has been tested on the adsorption of Basic Blue 41 from simulated dye polluted water. This dye, utilized in textile industries, has often been used as model pollutant in scientific studies (Kooli et al., 2015; Vinh and Bin, 2007). Preliminary results on $NiFe_2O_4$/kaolinite composite (obtained by using tartaric acid as fuel agent and a clay-to-ferrite mass ratio of 3:1) in the photocatalytic decomposition of another dye, MO, have been already published (Cojocaru et al., 2017), offering us the information that the magnetic composite materials of this type can be optimized through synthesis for becoming highly efficient in dye adsorption. Hence, the main objective of this paper is to optimize the microstructure, morphologies, textural and magnetic properties of nanocomposites by using different fuel agents and mass ratios of clay-to-nickel ferrite, for attaining a high adsorption of Basic Blue 41 dye from aqueous solutions.

## 2. Material and methods

### *2.1. Adsorbents synthesis and characterization*

The clay, originating from a natural Romanian deposit, was obtained commercially and used without additional chemical purification. The graded analytical reagents used to obtain the ferrite component of the composites were ferric nitrate $Fe(NO_3)_3$•$9H_2O$, nickel nitrate $Ni(NO_3)_2$•$6H_2O$, glycine ($C_2H_5NO_2$) and tartaric acid ($C_4H_6O_6$) as chelating/combustion agents, as purchased from Sigma-Aldrich. Basic Blue 41 (BB41) azo dye was provided by Merck Co.

The magnetic nanocomposite materials were obtained by *in situ* synthesis of magnetic nanoparticles through the sol-gel auto-combustion method. The metallic nitrates and chelating/combustion agent were dissolved in distilled water. Atomic ratio of $Ni^{2+}$:$Fe^{3+}$ metallic cations was 1:2. The metallic cations-to-fuel agent molar ratio was 1:1, and it can be taken as the fuel-deficient ratio ($\rho$ = ¾) (Borhan et al., 2013). A quantity of kaolin clay was then combined into the solution containing ferrite precursors, in a calculated 3:1, 4:1, 5:1 mass ratio of clay-to-nickel ferrite. The sol was stirred for 2.5 h at 350 rpm and 80 ºC in a water bath, until gelation was visible. The transformation into gel varied, depending on the chelating/combustion agents used and on the clay-to-ferrite mass ratio, as presented in Table 1.

Auto-combustion occurred when the temperature reached 200 ºC for samples with glycine, accompanied by flame, being rapid, lasting just a few seconds. For the one with tartaric acid, the auto-combustion started at 250 ºC, being slower and lasting 5 min. Heating of the grounded powders was continued at an increasing rate of 50 ºC/h up to 350 ºC. In this way, the cubic spinel structure stabilization of the ferrite increases gradually. In view of its analysis, testing and comparison, the natural clay (composite source) was heated at 350 °C (named C350). The purchased clay was suspended in the same amount of distilled water, magnetically stirred at 80 °C until the soil hardened as a result of gradual evaporation, and finally heated up to 350 °C, at a heating rate of 50°C/h.

**Table 1.** Synthesized materials and their symbols

| *Sample* | *Clay: $NiFe_2O_4$ mass ratio* | *Chelating / combustion agent* | *Gelling time (h)* | *Auto-combustion temperature (°C)* | *Heating temperature (°C)* |
|---|---|---|---|---|---|
| C3Ni_gly350 | 3 : 1 | Glycine | 2.5 | 200 | 350 |
| C4Ni_gly350 | 4 : 1 | Glycine | 1 | 200 | 350 |
| C5Ni_gly350 | 5 : 1 | Glycine | < 1 | 200 | 350 |
| C3Ni_act350 | 3 : 1 | tartaric acid | 2 | 250 | 350 |
| C350 | 1 : 0 | - | - | - | 350 |

Phase identification was realized using a Shimadzu LabX 6000 diffractometer equipped with graphite monochromator and CuKα radiation (λ=1.5406 Å) from 20 to 80º for the 2θ angle, at a scanning step of 0.02º/s. FT-IR spectra were obtained using a Bruker TENSOR TM27 with ATR cell, with a 2 $cm^{-1}$ resolution in the 4000-370 $cm^{-1}$ domain. Scanning electron microscopy (SEM), carried out on a Hitachi S2600N Microscope, provided micrographs of the nanocomposites. Transmission electron micrographs (TEM) were obtained on a TESLA 513A electron microscope. Nitrogen gas sorption was performed to obtain information regarding the texture of the nanocomposites at a temperature of 77K, using a Quantachrome Nova 2200. The magnetic properties of composites were studied under normal conditions of pressure and temperature, using a PMC MicroMag 3900 VSM magnetometer. Absorbance measurements of the dye solutions were performed with a PharmaSpec UV-1700 Shimadzu UV-Vis spectrophotometer.

### *2.2. Basic Blue 41 removal procedure*

The adsorptive properties of the mesoporous clay and nanocomposites were tested on the removal of Basic Blue 41 (BB41) dye ($C_{20}H_{26}N_4O_6S_2$) (Roulia and Vassiliadis, 2005) from an aqueous solution. The experiment was carried out a solution of BB41 azo dye with high concentration (400 mg/L), under normal conditions and in the presence of natural light, without any external stimulus. In a test tube, 0.4 mL BB41 stock solution was brought to an established volume with 10 mL of distilled water, to obtain BB41 sol, after which 0.4 mL of hydrogen peroxide ($H_2O_2$ 30%) and 20 mg of nanocomposite were added. The mixture was manually stirred in order to homogenize the solution and then left to rest for 2 h, 6 h, 12 h and 24 h, respectively. In this investigation, the adsorption experiments were conducted to the extreme using as little amount of adsorbent as possible (taking into account the textural properties of materials) and at a very high concentration of dye. To rule out any dye degradation due either to the influence of light or to the sole addition of $H_2O_2$, blank samples were analyzed. Thus, the following blank samples, without nanocomposites were prepared:

- Blank, containing the stock solution of dye and distilled water.
- Blank-$H_2O_2$, containing BB41 stock solution, distilled water and hydrogen peroxide (30%).
- Control System, consisting of dye solution and mesoporous nanocomposites, created to verify whether the addition of $H_2O_2$ enhances the removal rate of the dye. Dosing of the dye in solution was made after 24 hours of contact.

To investigate the change in the concentration of the solution, the absorbance of BB41 solutions was determined at 608 nm. The percentage of dye removed from the solution was calculated using the equation (Eq. 1):

$$Removal\ (\%) = \frac{C_i - C_e}{C_i} \times 100 \quad (1)$$

where: $C_i$ represents the initial concentration of the solution and $C_e$is the equilibrium concentration of the analyzed solution.

## 3. Results and discussion

### *3.1. Nanocomposites characterization*

The diffraction patterns of the clay and nanocomposites prepared are presented in Fig. 1.

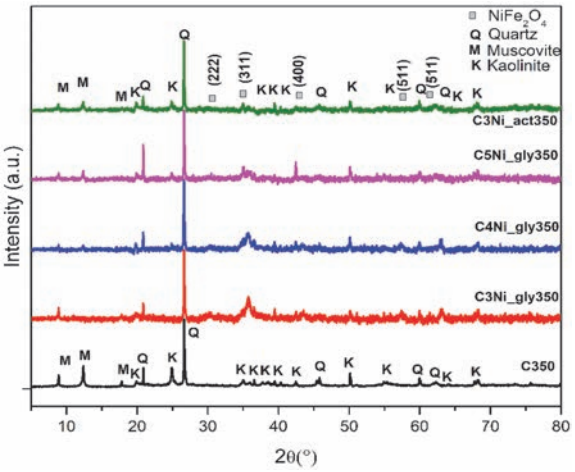


**Fig. 1.** X-ray diffraction patterns of the adsorbents

The crystalline phases of both clay and nickel ferrite have been identified. Previous studies (Cojocaru et al., 2015, 2017) have identified the raw clay used to synthesize the composite as being of kaolin type, with three crystalline species present in the crude clay: kaolinite, muscovite and quartz. Kaolinite mineral is recognized through the presence of clearly distinguished diffraction peaks at 12.37° and 26° values of 2$\theta$ (Cojocaru et al., 2015; Benea and Gorea, 2004), according to the JPCDS 75-1593 card. The peaks observed at 8.8° and 17.8° are associated with the presence of muscovite in the sample, while the ones found at 20.7°, 26.6° and 59.9° - with the presence of quartz (Duarte-Silva et al., 2014). The high intensity of peaks, attributed to quartz specie, reveals it as the dominant mineral present in the samples, with a large quartz impurity.

The reflection peaks corresponding to nickel ferrite are also visible in the diffraction pattern, although their intensities are lower, due to the low heating temperature of nanocomposites of 350 °C and the low quantity of ferrite. The reflection peak found at 35.72° (2θ) is attributed to the (3 1 1) plane, characteristic to the cubic spinel structure with space group Fd3m (Dumitrescu et al., 2013; Shanmugavel et al., 2015). The diffraction peaks were identified and indexed in good agreement with JCPDS 89-4927 and 89-4926, provided by the International Centre for

Diffraction Data (ICDD) data base. Thus, a temperature of 350 °C was sufficient for the successful insertion of the $NiFe_2O_4$ phase in the structure of kaolin clay, as also confirmed by SEM and TEM.

The ratio of nickel ferrite relatively to clay was mathematically calculated. The percentage of ferrite obtained may be different from the theoretical one, because of its development in both clay pores and on the surface, or because of the extremely violent auto-combustion process. The quantity ($Qty_{NiF}$) of the ferrite from the composites was established taking into account the height of the main peak ($H_Q$) corresponding to the quartz phase, and that of the peak (311) corresponding to ferrite ($H_{NiF}$), based on the relation (Eq. 2):

$$Qty_{NiF} = \frac{H_{NiF}}{H_{NiF} + H_Q} \times 100 \quad (2)$$

The percentage closest to the estimated one is for C4Ni_gly350. The difference can be canceled by another temperature rise. In the case of C3Ni_act350, the calculated $NiF_2O_4$ quantity was of 10%, which means that only 40% of ferrite is present in the composite. By comparing this sample with C3Ni_gly350, C4Ni_gly350 and C5Ni_gly350, it can be seen that the composite materials synthesized with glycine resulted in a more intense development of the spinel structure, at the same temperature of 350 °C. An explanation is the temperature at which the flame reaches auto-combustion, namely 505 °C for tartaric acid and 1200 °C, respectively, for glycine (Druc et al., 2013; Srinivasan et al., 1984). Slight variations in the diffraction peak positions, depending on the clay-to-ferrite ratio and fuel agents, are observed. Thus, the XRD data were used to estimate the lattice parameters, crystallite size and X-ray density of the studied powders (Table 2). The lattice parameter $a_{311}$ and the crystallite size ($D_{DS}$) of the nanocomposites were determined according to Laue and Debye-Scherrer equations for cubic lattice (Eqs. 3-4):

$$\alpha_{311} = d_{311}(h^2 + k^2 + l^2)^{1/2} \quad (3)$$

$$D_{DS} = \frac{0.9\lambda}{\beta \cos\theta} \quad (4)$$

where: $D_{DS}$ is the mean dimension of the crystallite perpendicular to the miller plane (*hkl*), $\lambda$ is the wavelength of the X-ray source used ($K\alpha$ = 1.5406 Å), $\beta$ is the full width at half maximum of the diffraction (3 1 1) in radians and $\theta$is the Braggs angle. A Gaussian fitting model was used with maximum estimated errors ±0.5% for $\beta$ values and±0.2% for $\theta$ values. The values of the X-ray density ($d_x$) were calculated according to the (Eq. 5):

$$d_x = \frac{ZM}{Na^3} \quad (5)$$

where: $Z$ is the number of molecules per primitive unit cell (Z=8), $M$ is the molecular weight of each composite and $N$ is Avogadro's number (6.0223 x $10^{23}$ particles/mol).

Estimated crystallite size revealed that the temperature attained in auto-combustion plays an important role. Also, the crystallite size decreased with the clay-to-ferrite ratio increase, while the auto-combustion time decreased. The composite synthesized with tartaric acid C3Ni_act350 have a smaller size of the lattice parameter, $D_{DS}$ and $d_x$, compared to C3Ni_gly350, due to the lower temperature attained during auto-combustion. The small crystallite size indicates large specific surface areas, which should lead to significant catalytic and adsorptive performances.

FT-IR absorption spectra of the prepared compounds, recorded in the 4000 - 350 $cm^{-1}$ range, are shown in Fig. 2. Absorption bands corresponding to clay and ferrite can be observed, confirming the successful inclusion of nickel ferrite into the structure of kaolin clay. Based on data previously reported in literature (Armijo, 1969; Srinivasan et al., 1984; Srivastava et al., 2009), the development of the cubic spinel structure characteristic to ferrite can be observed in the 600 - 400 $cm^{-1}$ range. The bands which appear between 570 - 550 $cm^{-1}$ correspond to intrinsic stretching vibrations of the metal-oxygen bond located in the tetrahedral sites of the ferrite lattice ($\upsilon_1$). The weaker absorption maxima at around 425 $cm^{-1}$ are attributed to the stretching vibrations of the metal-oxygen bonds situated in octahedral sites ($\upsilon_2$) (Nejati and Zabihi, 2012). The bands located at 1635$cm^{-1}$, 2852$cm^{-1}$ and 2923 $cm^{-1}$ are assigned to C-H vibrations (Pradeep et al., 2008), which indicates the presence of organic impurities in the structure of ferrite. The presence of an organic phase was to be expected, given the low heating temperature to which the composites were subjected. Absorption bands characteristic to kaolin clay appear due to the vibrations of bonds between O-H, Si-O and Al-OH (Cojocaru et al., 2015; Saikia et al., 2003).

**Table 2.** Experimental and calculated XRD data obtained for powders heated at 350 °C

| ***Sample*** | $Qty_{NiFe2O4(th)}$ ***(%)*** | $Qty_{NiFe2O4(XRD)}$ ***(%)*** | $D_{DS}$ ***(%)*** | $a_{311}$ ***(Å)*** | $d_x$ ***(g/cm³)*** |
|---|---|---|---|---|---|
| C350 | 0 | 0 | 763 | - | - |
| C3Ni_gly350 | 25 | 15.3 | 198 | 8.32 | 5.40 |
| C4Ni_gly350 | 20 | 12.9 | 171 | 8.33 | 5.37 |
| C5Ni_gly350 | 16.6 | 8.30 | 31 | 8.32 | 5.31 |
| C3Ni_act350 | 25 | 10.0 | 39 | 8.31 | 5.38 |

The bands appearing between 3620 and 3700 $cm^{-1}$ are generated by in-phase symmetric stretching vibration of O-H bonds. Si-O deformation bonds appear in the 1120 - 1000 $cm^{-1}$ range and Si-O stretching bonds are visible at 795, 755 and 696 $cm^{-1}$ (Ekosse, 2005).

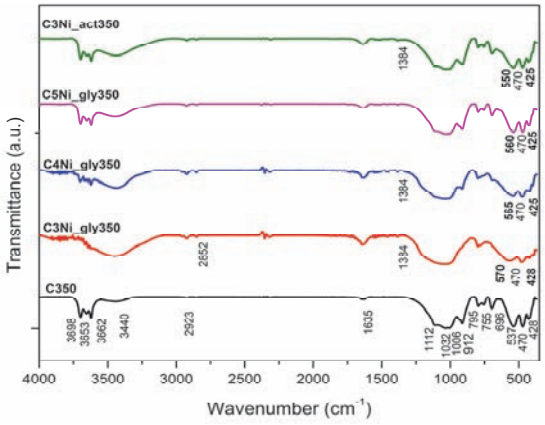


**Fig. 2.** IR spectra of adsorbents

The SEM images of C350 clay and mesoporous nanocomposites are shown in Figs. 3 (a-e). The lamellar internal structure of the clay fraction is visible. The gas release in the auto-combustion stage of the synthesis process is responsible for the creation of the holes visible in the images. Nickel ferrite appears to be formed on the surface of the clay, and an agglomeration of $NiFe_2O_4$ nanoparticles with irregular morphology of aggregates is observed, as confirmed by the TEM image (Fig. 3f) of C3Ni_gly350. Hence, $NiFe_2O_4$ pseudo-cubic nanoparticles have been distributed into clusters and located outside clay interlayer spaces, which led to the formation of a mesoporous architecture by stacking of clay layers, as confirmed by $N_2$ physisorption analysis.

The nitrogen adsorption-desorption isotherms for the adsorbents obtained at 77 k are shown in Fig. 4. According to the IUPAC classification, the obtained isotherm is of type IV, with a H3 hysteresis loop (Sing, 1982), which indicates non-uniform size pores and a mesoporous structure of nanocomposites (Walerczyk et al., 2012). The data obtained from physisorption of nitrogen was used to determine BET and Langmuir surface areas. According to the BJH method, the cumulative volume of pores and average pores width are shown in Table 3. C350 clay has a $S_{BET}$ surface area of 31 $m^2/g$ and an average pore diameter between 8.1 and 9.0 nm (calculated from desorption and adsorption isotherms, respectively), indicating a good adsorption capacity of the dye. C3Ni_act350 has the highest $S_{BET}$ and Langmuir surface area, of 67 and 94 $m^2/g$, respectively. Observed here is the influence of the fuel agent used and of the thermal treatment applied on the textural characteristics of nanocomposites. The low flame temperature generated by tartaric acid at the time of auto-combustion favors a slower spinel structure development and, therefore, a smaller size of crystallites. Similarly, heating at only 350 °C leads to a larger specific surface area. On the opposite side, there is the C4Ni_gly350 nanocomposite, characterized by a $S_{BET}$ value of 29 $m^2/g$ and 41 $m^2/g$ for the Langmuir surface area, values about 60% lower than those of C3Ni_act350. The higher flame temperature generated by glycine during the auto-combustion process (up to 1200 °C) favors the rapid development of spinel structure, the increase of crystallinity and, therefore, the decrease of the specific surface areas, which agrees with the XRD results.

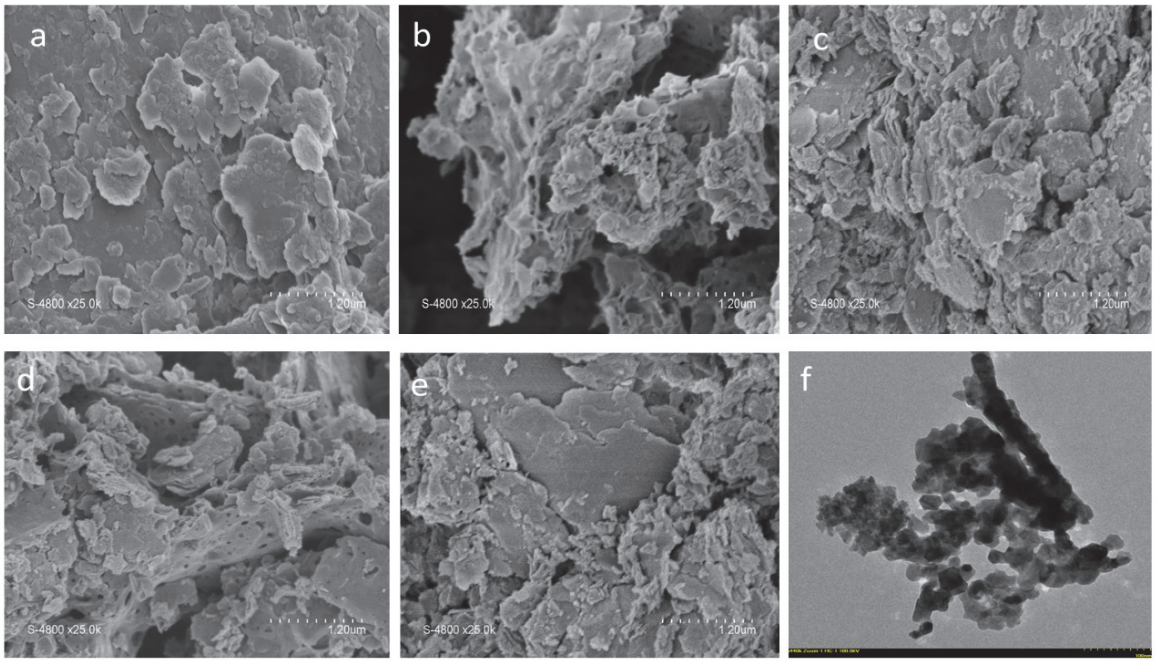


**Fig. 3.** SEM micrographs of clay and magnetic composites (a-e) and TEM image of C3Ni_gly350 (f)

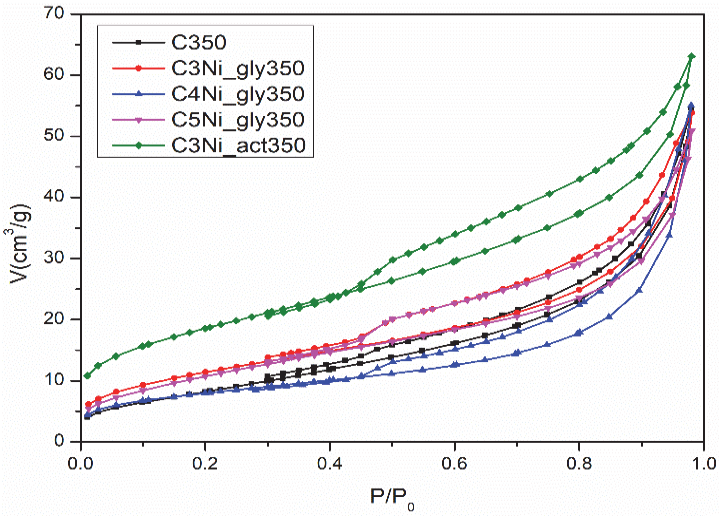


**Fig. 4.** Nitrogen adsorption-desorption isotherms of adsorbents

**Table 3.** Textural properties of adsorbents

| *Sample* | *BET surface area ($m^2/g$)* | *Langmuir surface area ($m^2/g$)* | *Volume of pores (Adsorption) ($cm^3/g$)* | *Volume of pores (Desorption) ($cm^3/g$)* | *Average pore width (Adsorption) (nm)* | *Average pore width (Desorption) (nm)* |
|---|---|---|---|---|---|---|
| C350 | 31 | 45 | 0.08 | 0.07 | 9.00 | 8.11 |
| C3Ni_gly350 | 42 | 60 | 0.08 | 0.07 | 8.30 | 7.40 |
| C4Ni_gly350 | 29 | 41 | 0.08 | 0.07 | 12.9 | 9.67 |
| C5Ni_gly350 | 40 | 58 | 0.07 | 0.07 | 8.00 | 6.80 |
| C3Ni_act350 | 67 | 94 | 0.09 | 0. 08 | 6.01 | 6.16 |

Although can be interpreted as a decrease in the adsorptive properties of the synthesized material, composite shows the highest values of the mean pore diameter - of 12.9 nm for adsorption and of 9.67 nm, respectively, for desorption. As clay does not naturally exhibit magnetism, the insertion of Ni ferrite into the clay allows it to develop magnetic properties (Maaz et al., 2010). The hysteresis loop of one composite, C5Ni_gly350, plotted in Fig. 5, presents a very narrow cycle, typical for soft magnetic materials (Nejati and Zabihi, 2012).

The slim "S" shape of the loop also suggests that the composite presents a soft ferromagnetism. All materials present the same shape of cycle; magnetization data are presented in Table 4. The values of the coercitive field and the remanent magnetization indicate that the composites are in a superparamagnetic state, meaning that it can easily be demagnetized after removing the applied magnetic field, which is a huge advantage in their application as magnetic adsorbent materials for organic pollutants in water, easily separable from the solution. Because magnetic saturation was not reached during measurements, the computed Ms values were determined by extrapolation of the magnetic field to infinity, in the representation of Ms as function of 1/H. The low values of saturation magnetization at 10 kOe are related to the small amount of nickel ferrite in clay, as well as to the irregular crystalline structure of the magnetic phase in nanocomposites.

### *3.2. Adsorption studies*

#### *3.2.1. Dye removal by adsorbents*

The adsorption efficiency of aqueous Basic Blue 41 dye induced by treated clay and novel magnetic nanocomposites, depending on time, in the presence of $H_2O_2$ (2, 6, 12 and 24 hours respectively) and absence of $H_2O_2$ (24 hours - Control System) was investigated. The UV-Vis spectra of the five prepared samples are shown in Fig. 6. The increase of contact time from 2 to 24 hours significantly increases the percentage of adsorbed dye for all samples. As shown in Fig. 7, the Blank and Blank-$H_2O_2$ samples show no changes in concentration after different contact times, the conclusion being that subsequent removal of the dye was strictly due to the action of the synthesized mesoporous nanocomposites in the presence of hydrogen peroxide. The performance of clay sample C350 is significant, as it manages to remove, within 2 hours, 97% of BB41 dye from the solution. The best-performing composite material is C3Ni_act350, that removed 98% of the BB41 dye from the solution within 24 hours. Also, it can be stated that the removal rate increases linearly with increasing the clay-to-ferrite mass ratio.

**Table 4.** Magnetic properties of adsorbents

| ***Sample*** | ***Specific magnetization at 10kOe (M) emu/g*** | ***Saturation magnetization (Ms) emu/g*** | ***Coercivity (Hc) Oe*** | ***Remanent magnetization (Mr) emu/g*** |
|---|---|---|---|---|
| C350 | 0.04 | 0.06 | 185 | 0.004 |
| C3Ni_gly350 | 5.10 | 8.80 | 30 | 0.340 |
| C4Ni_gly350 | 4.30 | 7.80 | 26 | 0.283 |
| C5Ni_gly350 | 1.40 | 1.70 | 16 | 0.063 |
| C3Ni_act350 | 3.10 | 5.50 | 11 | 0.091 |

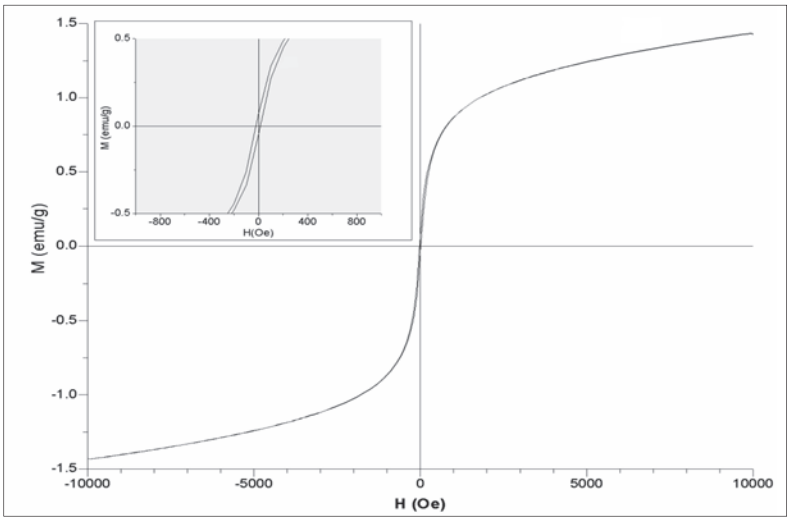


**Fig. 5.** Magnetization curve of C5Ni_gly350 magnetic composite

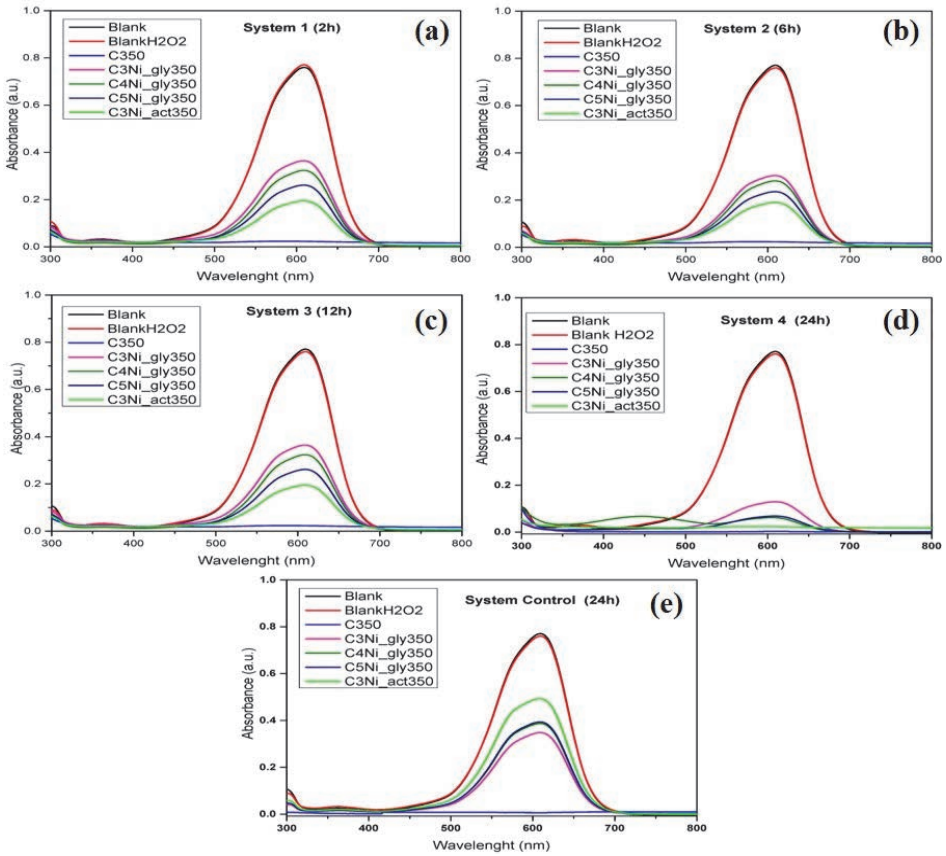


**Fig. 6.** Changes in the UV-Vis spectra of BB41 in the presence of adsorbents and $H_2O_2$ after different contact time: System 1 (2h): after 2 hours; (b) System 2 (6h): after 6 hours; (c) System 3 (12h): after 12 hours; (d) System 4 (24h): after 24 hours; (e) System Control: Stock solution BB41 - distilled water - powders after a contact time of 24 hours

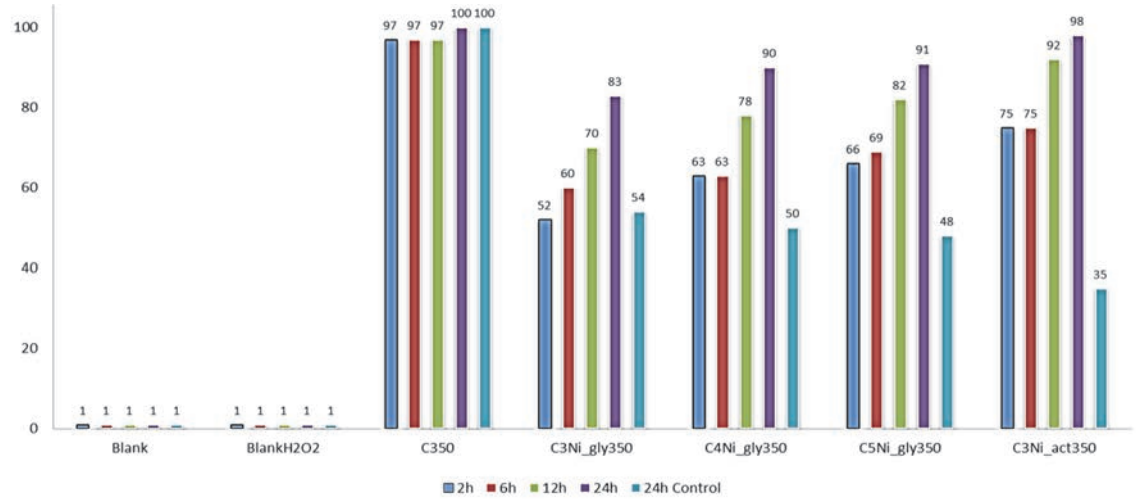


**Fig. 7.** Percentage of BB41 dye removed by all adsorbents

*3.2.2. Effect of $H_2O_2$ on discoloration efficiency*

Improvement of discoloring efficiency in the presence of hydrogen peroxide in systems is evident. Kharisov et al. (2014) and Debecker et al. (2013) have shown that addition of hydrogen peroxide - as an oxidizing agent - improves the speed of a catalytic reaction. Hence, the presence of $H_2O_2$ in solutions leads to the formation of free radicals which accelerate up the removal process of the dye, due to the increase of the electronic exchange $Fe^{2+} \leftrightarrow Fe^{3+}$ on the ferrite active sites.

Increase in the percentage of dye adsorbed from the solution by the magnetic nanocomposites prepared with glycine, after a 24 hour contact time, from ~ 48% in the case of Control System (without $H_2O_2$), to ~ 91% (in presence of $H_2O_2$), shows that the presence of hydrogen peroxide in the solution has almost doubled the quantity of dye retained. In the case of C3Ni_act350 nanocomposite, the removal rate of BB41 increases three times, from 35% to 98%. This also indicates that the chemical processes causing the removal of BB41 were both adsorption and catalytic, as $H_2O_2$ is not known to improve the adsorptive properties of clay, having no effect of its own on the degradation of BB41. Finally, by using an external magnetic field, the composite was removed from the solution, which proves that the objective of the research was accomplished (Fig. 8).

*3.2.3. Effect of contact time on the adsorption capacity*

Fig. 9 (a) shows the effect of contact time on the adsorption capacity of BB41 dye onto both clay C350 and magnetic composites. It can be seen that the adsorption process for C350 clay could be divided into two steps and, for the rest of composites, into three steps. In the first step, the adsorption capacity of BB41 is 717.8 mg/g onto C350. With the introduction of a magnetic component in the system, the adsorption capacities (Table 5) of BB41 were reduced to 385 mg/g for C3Ni_gly350. However, the maximum adsorption capacity, of 752.2 mg/g, was obtained for C3Ni_act350, followed by a second slow step, reaching 740 mg/g after 12 h.

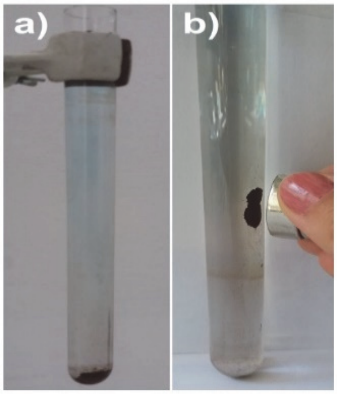


**Fig. 8.** (a) Removal of BB41 in the presence of C3Ni_act350 adsorbent and $H_2O_2$and (b) Removing magnetic C3Ni_act350 composite from the solution after 24h using a magnet

In the third step, the rate of BB41 adsorption on magnetic composites was slow, reaching equilibrium at about 24 h. More precisely, the adsorption capacity of magnetic composites increased with increasing the $NiFe_2O_4$ content, as a function of the fuel agents employed.

## 5. Adsorption kinetics modeling and mechanism

*5.1. Pseudo-second order kinetic model*

Adsorbent's capacity and its removal performance increase with contact time. Pseudo-second order kinetic (Ho and McKay, 1998) and intra-particle diffusion models (Annadurai et al., 2002) Yu et al., 2018;were applied to fit the experimental data from the adsorption of BB41 onto adsorbents. The pseudo-second order model was well-fitted to the kinetic results of BB41 (Fig. 9(b)). In the literature, adsorption kinetics of many dye species onto various adsorbents was also fitted to a pseudo-second order

(Dalvand et al., 2016; Keyhanian et al., 2016; Kausar et al., 2018; Liu et al., 2015; Tao et al., 2016). These models can be expressed as (Eqs. 6-7):

$$\frac{t}{qt} = \frac{1}{K_2 q_{2e}^2} + \frac{t}{q_{2e}} \quad (6)$$

$$q_t = K_3 t^{1/2} \quad (7)$$

where: $q_{2e}$ and $q_t$ (mg/g) are the adsorption capacity of BB41 at equilibrium and at time t (min), respectively, $K_2$ (g/mg·min) is the adsorption rate constant of the second-order equation, $K_3$ (mg/g·min$^{1/2}$) is the intra-particle diffusion rate constant. Constants $k_2$, $q_{2e}$ and the correlation coefficients ($R^2$), directly obtained from the intercept and slope of the plot of t/$q_t$*versus* t, are given in Table 5. The $q_{2e}$ values determined from the model, along with the correlation coefficients, were very close to qt, while the correlation coefficient was closer or higher than 0.99, depending on the kaolin-to-ferrite mass ratio. As a matter of consequence, the adsorption process of BB41 could be well-described by the pseudo-second-order model. This adequate model shows that adsorption of BB41 onto the studied adsorbents is controlled by a chemisorption mechanism, which confirmed that it takes place probably *via* surface exchange reactions, until the surface functional sites are fully occupied.

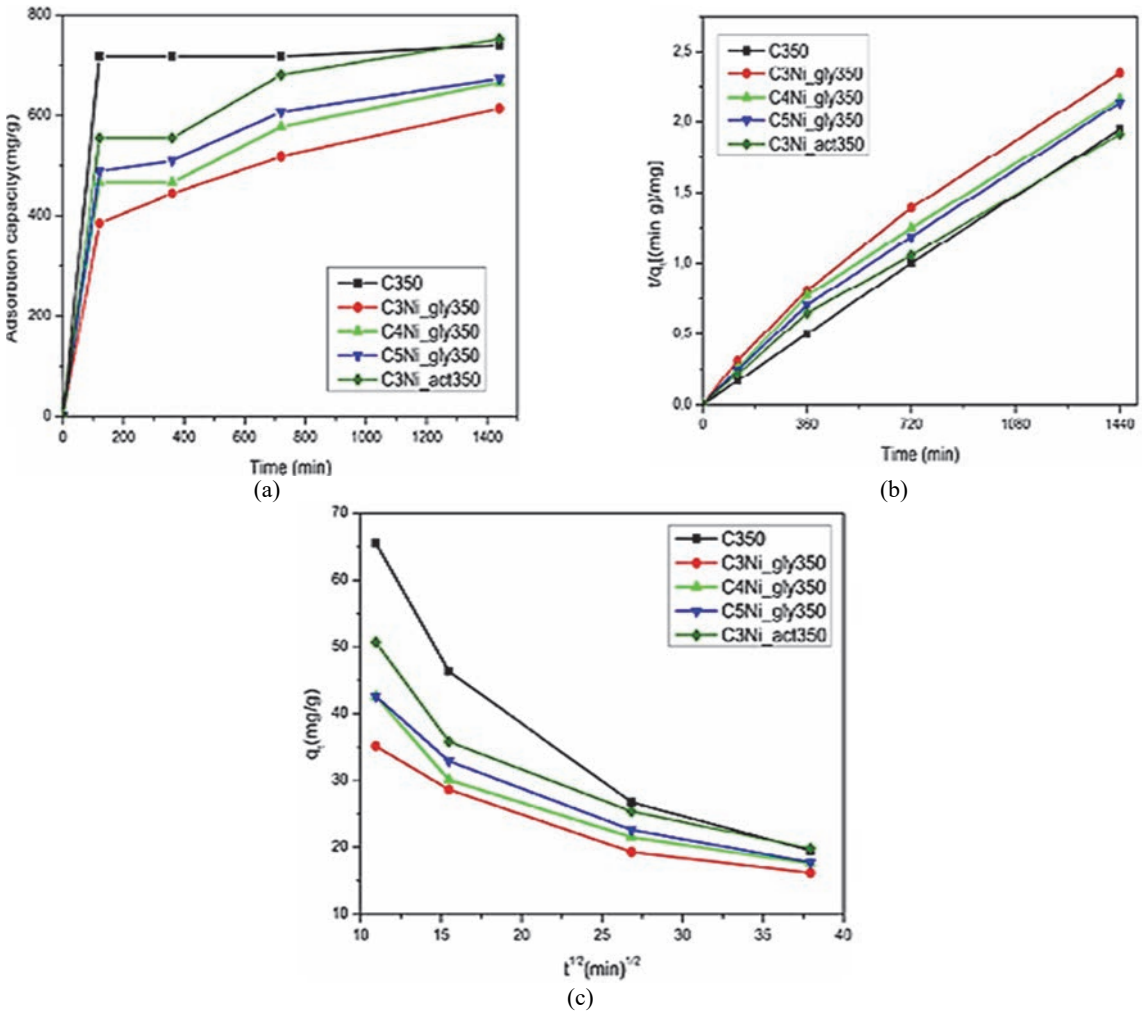


**Fig. 9.** (a) Effect of contact time on the adsorption capacity of BB41 by adsorbents, (b) Pseudo-second-order kinetic model for the adsorption of BB41, (c) Intra-particle-diffusion model for the adsorption of BB41

**Table 5.** Kinetic parameters for the adsorption of BB41 onto kaolin clay and magnetic composites

| *Sample* | *Pseudo-second order rate equation* | | | | | *Intra-particle diffusion model* | |
|---|---|---|---|---|---|---|---|
| | $q_t$ (mg/g) | (%) | $q_{2e\ (cal)}$ (mg/g) | $K_2$ (g/mg min) | $R^2$ | $K_3$ (mg/g min$^{1/2}$) | $R^2$ |
| C350 | 717.80 | 100 | 741 | $1.95\times10^{-4}$ | 0.9996 | 39.53 | 0.736 |
| C3Ni_gly350 | 614.20 | 83 | 625 | $3.19\times10^{-5}$ | 0.9986 | 24.82 | 0.768 |
| C4Ni_gly350 | 666.00 | 90 | 680 | $2.89\times10^{-5}$ | 0.9915 | 27.93 | 0.690 |
| C5Ni_gly350 | 673.00 | 91 | 684 | $3.97\times10^{-5}$ | 0.9905 | 29.47 | 0.783 |
| C3Ni_act350 | 752.20 | 98 | 763 | $3.30\times10^{-5}$ | 0.9985 | 32.92 | 0.720 |

*5.2. Intra-particle-diffusion model*

The plots of qt *versus* $t^{1/2}$ for all adsorbents represented in Fig. 9(c) showed multi-linearity, signifying that multiple stages were involved in the adsorption process. The intra-particle-diffusion coefficients $K_3$ for all adsorbents under study were calculated from the slope of the corresponding linear region plotted in Fig. 9(c), being listed in Table 5.

The first two straight portions can be attributed to surface diffusion and the last linear section - to mesopores diffusion. Hence, the BB41 dye molecules were transported to the external surface of the nanocomposite particles through surface diffusion, at a relatively fast rate, after which the dye molecules entered into particles by intra-particle diffusion through the pores. The plotted lines did not pass through the origin, indicating that external surface diffusion and intra-particle diffusion occurred simultaneously.

## 6. Conclusions

Ultra-effective magnetic $NiFe_2O_4$/kaolin clay adsorbents with a high adsorption capacity and good magnetic separation performance were successfully prepared by sol-gel auto-combustion method. The magnetic phase formed in the composites is spinel type oxide $NiFe_2O_4$. The magnetic composites synthesized with glycine resulted in deeper development of the spinel structure at the temperature of 350 °C, confirmed also by SEM and TEM analysis.

The textural properties of the mesoporous materials, corroborated with those obtained from the XRD, SEM and TEM suggest that the magnetic Ni ferrite/kaolin composites can be successfully used as adsorbents in the removal of dyes from wastewater. The obtained composites have smaller adsorption properties in comparison with kaolin clay because of the stabilization of Ni ferrite nanoparticles in the clay mesopores and not on the surface and with increasing ion strength, adsorption capacity decreased due to screening of the surface charges.

The adsorption kinetic data can be described by the second-order kinetic model, which confirmed that adsorption of BB41 takes place via surface exchange reactions until the surface functional sites are fully occupied. The adsorption capacity of BB41 was 717.8 mg/g onto C350. Then, it was reduced to 385 mg/g for C3Ni_gly350 and finally, the maximum saturation capacity of 752.2 mg/g was obtained for C3Ni_act350, which showed that fuel agent and textural properties play an important role in adsorption performance. Hence, the adsorption capacity of magnetic composites increased with increasing $NiFe_2O_4$ content and depends on the fuel agents. It was also proven that the best removal results are achieved when both composite and hydrogen peroxide are present in solution.

Increasing the contact time between the composite and solution, from 2 hours to 24 hours leads to a growth in the rate of BB41 adsorbed, from 52 to 98%. It was shown that magnetic composite adsorbents were easily and effectively removed from the solution by magnetic separation.

**Acknowledgments**

This work was supported by a grant of Ministry of Research and Innovation, CNCS - UEFISCDI, project number PN-III-P1-1.1-PD-2016-1510, within PNCDI III. This work was supported by the strategic grant POSDRU/159/1.5/S/133391, Project "Doctoral and Post-doctoral programs of excellence for highly qualified human resources training for research in the field of Life sciences, Environment and Earth Science", co-financed by the European Social Fund within the Sectorial Operational Program Human Resources Development 2007 - 2013.

## References

Ai L., Zhou Y., Jiang J., (2011), Removal of methylene blue from aqueous solution by montmorillonite/$CoFe_2O_4$ composite with magnetic separation performance, *Desalination*, **266**, 72-77.

Annadurai G., Juang R.S., Lee D.J., (2002), Use of cellulose-based wastes for adsorption of dyes from aqueous solutions, *Journal of Hazardous Materials*, **92**, 263-274.

Armijo J.S., (1969), The kinetics and mechanism of solid-state spinel formation - A review and critique, *Oxidation of Metals*, **1**, 171-198.

Benea M., Gorea M., (2004), Mineralogy and technological properties of some kaolin types used in the ceramic industry, *Studia UBB Geologia*, **49**, 33-39.

Borhan A.I., Slatineanu T., Iordan A.R., Palamaru M.N., (2013), Influence of chromium ion substitution on the structure and properties of zinc ferrite synthesized by the sol-gel auto-combustion method, *Polyhedron*, **56**, 82-89.

Bourlinos A.B., Devlin E., Boukos N., Simopoulos A., Petridis D., (2002), Magnetite and Co ferrite-based clay composites, *Clay Minerals*, **37**, 135-141.

Cojocaru S., Borhan A.I., Mykhailovych V., Cucu-Man S., Melniciuc-Puica N., Călţun O.F., Hulea V., Cazacu M., Palamaru M.N., Iordan A.R., (2017), Nanosized $NiFe_2O_4$/Kaolinite composite as adsorbent for organic dyes, *Revue Roumaine de Chimie*, **62**, 687-698.

Cojocaru S., Dumitrescu A.M., Breaban I.G., Domocos A.A., Iordan A.R., Melniciuc-Puica N., Palamaru M.N., (2015), Exploiting the natural potential of romanian kaolin clay. Adsorption capacity improvement through heat treatment, *Optoelectronics and Advanced Materials-Rapid Communications*, **9**, 1530-1534.

Dalvand A., Nabizadeh R., Ganjali M.R., Khoobi M., Nazmara S., Mahvi A.H., (2016), Modeling of Reactive Blue 19 azo dye removal from colored textile wastewater using L-arginine-functionalized $Fe_3O_4$ nanoparticles: Optimization, reusability, kinetic and equilibrium studies, *Journal of Magnetism and Magnetic Materials*, **404**, 179-189.

Debecker D.P., Hulea V., Mutin P.H., (2013), Mesoporous mixed oxide catalysts via non-hydrolytic sol-gel: a review, *Applied Catalysis A: General*, **451**, 192-206.

Druc A.C., Dumitrescu A.M., Borhan A.I., Nica V., Iordan A.R., Palamaru M.N., (2013), Optimization of synthesis conditions and the study of magnetic and dielectric properties for $MgFe_2O_4$ ferrite, *Open Chemistry*, **11**, 1330-1342.

Duarte-Silva R., Villa-García M.A., Rendueles M., Díaz M., (2014), Structural, textural and protein adsorption properties of kaolinite and surface modified kaolinite adsorbents, *Applied Clay Science*, **90**, 73-80.

Dumitrescu A.M., Samoila P.M., Nica V., Doroftei F., Iordan A.R., Palamaru M.N., (2013), Study of the chelating/fuel agents influence on $NiFe_2O_4$ samples with potential catalytic properties, *Powder Technology*, **243**, 9-17.

Ekosse G.I.E., (2005), Fourier transform infrared spectrophotometry and X-ray powder diffractometry as complementary techniques in characterizing clay size fraction of kaolin, *Journal of Applied Sciences and Environmental Management*, **9**, 43-48.

Hao L., Liu M., Wang N., Li, G., (2018), A critical review on arsenic removal from water using iron-based adsorbents, *RSC Advances*, **8**, 39545-39560.

Hashem F.S., (2012), Adsorption of Methylene Blue from Aqueous Solutions using $Fe_3O_4$/ Bentonite Nanocomposite, *Scientific Reports*, **1**, 1-549.

Hashemian S., (2011), Removal of Acid Red 151 from water by adsorption onto nano-composite $MnFe_2O_4$/kaolin, *Main Group Chemistry*, **10**, 105-114.

Ho Y.S., McKay G., (1998), Sorption of dye from aqueous solution by peat, *Chemical Engineering Journal*, **70**, 115-124.

Joshi S., Sharma M., Kumari A., Shrestha S., Shrestha, B., (2019), Arsenic removal from water by adsorption onto iron oxide/nano-porous carbon magnetic composite, *Applied Sciences*, **9**, 3732-3744.

Kanwal A., Bhatti H.N., Iqbal M., Noreen S., (2017), Basic dye adsorption onto clay/$MnFe_2O_4$ composite: a mechanistic study, *Water Environment Research*, **89**, 301-311.

Kaur M., Singh M., Mukhopadhyay S.S., Singh D., Gupta M., (2015), Structural, magnetic and adsorptive properties of clay ferrite nanocomposite and its use for effective removal of Cr (VI) from water, *Journal of Alloys* and *Compounds*, **653**, 202-211.

Kausar A., Iqbal M., Javed A., Aftab K., Bhatti H.N., Nouren S., (2018), Dyes adsorption using clay and modified clay: A review, *Journal of Molecular Liquids*, **256**, 395-407.

Keyhanian F., Shariati S., Faraji M., Hesabi M., (2016), Magnetite nanoparticles with surface modification for removal of methyl violet from aqueous solutions, *Arabian Journal of Chemistry*, **9**, 348-354.

Kharisov B.I., Dias H.R., Kharissova O.V., (2014), Mini-review: Ferrite nanoparticles in the catalysis, *Arabian Journal of Chemistry*, **12**, 1234-1246.

Kooli F., Liu Y., Al-Faze R., Al Suhaimi A., (2015), Effect of acid activation of Saudi local clay mineral on removal properties of basic blue 41 from an aqueous solution, *Applied Clay Science*, **116**, 23-30.

Liu Y., Zeng G., Tang L., Cai Y., Pang Y., Zhang Y., Yang G., Zhou Y., He X., He Y., (2015), Highly effective adsorption of cationic and anionic dyes on magnetic Fe/Ni nanoparticles doped bimodal mesoporous carbon, *Journal* of *Colloid and Interface Science*, **448**, 451-459.

Maaz K., Mumtaz A., Hasanain S.K., Bertino M.F., (2010), Temperature dependent coercivity and magnetization of nickel ferrite nanoparticles, *Journal of Magnetism and Magnetic Materials*, **322**, 2199-2202.

Makarchuk O.V., Dontsova T.A., Astrelin I.M., (2016), Magnetic nanocomposites as efficient sorption materials for removing dyes from aqueous solutions, *Nanoscale Research Letters*, **11**, 161.

Mehta D., Mazumdar S., Singh S.K., (2015), Magnetic adsorbents for the treatment of water/wastewater-A review, *Journal of Water Process Engineering*, **7**, 244-265.

Mohagheghian A., Pourmohseni M., Vahidi-Kolur R., Yang J-K., Shirzad-Siboni M., (2017), Application of kaolin-$Fe_3O_4$ nano-composite for the removal of azo dye from aqueous solutions, *Desalination* and *Water Treatment*, **58**, 308-319.

Nejati K., Zabihi R., (2012), Preparation and magnetic properties of nano size nickel ferrite particles using hydrothermal method, *Chemistry Central Journal*, **6**, 23.

Oliveira L.C., Rios R.V., Fabris J.D., Sapag K., Garg V.K., Lago R.M., (2003), Clay-iron oxide magnetic composites for the adsorption of contaminants in water, *Applied Clay Science*, **22**, 169-177.

Peng K., Fu L., Yang H., Ouyang J., (2016), Perovskite $LaFeO_3$/montmorillonite nanocomposites: synthesis, interface characteristics and enhanced photocatalytic activity, *Scientific Reports*, **6**, 19723.

Pradeep A., Priyadharsini P., Chandrasekaran G., (2008), Sol-gel route of synthesis of nanoparticles of $MgFe_2O_4$ and XRD, FTIR and VSM study, *Journal of Magnetism and Magnetic Materials*, **320**, 2774-2779.

Qu X., Alvarez P.J., Li Q., (2013), Applications of nanotechnology in water and wastewater treatment, *Water Research*, **47**, 3931-3946.

Roulia M., Vassiliadis A.A., (2005), Interactions between CI Basic Blue 41 and aluminosilicate sorbents, *Journal* of *Colloid* and *Interface Science*, **291**, 37-44.

Safarik I., Horska K., Svobodova B., Safarikova M., (2012), Magnetically modified spent coffee grounds for dyes removal, *European Food Research* and *Technology*, **234**, 345-350.

Safarik I., Safarikova M., (2010), Magnetic fluid modified peanut husks as an adsorbent for organic dyes removal, *Physics Procedia*, **9**, 274-278.

Saikia N.J., Bharali D.J., Sengupta P., Bordoloi D., Goswamee R.L., Saikia P.C., Borthakur P.C., (2003), Characterization, beneficiation and utilization of a kaolinite clay from Assam, India, *Applied Clay Science*, **24**, 93-103.

Saravanan A., Senthil Kumar P., Yaashikaa P.R., (2020), *Treatment of Dye Containing Wastewater Using Agricultural Biomass Derived Magnetic Adsorbents* In: *Green Materials for Wastewater Treatment. Environmental Chemistry for a Sustainable World*, Naushad M., Lichtfouse E. (Eds.), Springer, vol. 38, 149-169.

Shanmugavel T., Raj S.G., Kumar G.R., Rajarajan G., Saravanan D., (2015), Cost effective preparation and characterization of nanocrystalline nickel ferrites ($NiFe_2O_4$) in low temperature regime, *Journal of King Saud University - Science*, **27**, 176-181.

Sharma M., Kalita P., Senapati K.K., Garg A., (2018), *Study on Magnetic Materials for Removal of Water Pollutants*, In: *Emerging Pollutants: Some Strategies for the Quality Preservation of Our Environment*, Soloneski S., Larramendy M.L. (Eds.), IntechOpen, 61-78.

Sing K.S.W., (1982), Reporting physisorption data for gas/solid systems with special reference to the determination of surface area and porosity (Provisional), *Pure and Applied Chemistry*, **54**, 2201-2218.

Sivashankar R., Sathya A.B., Vasantharaj K., Sivasubramanian V., (2014), Magnetic composite an

environmental super adsorbent for dye sequestration - A review, *Environmental Nanotechnology*, *Monitoring and Management*, **1-2**, 36-49.

Srinivasan T.T., Srivastava C.M., Venkataramani N., M.J. Patni, (1984), Infrared absorption in spinel ferrites, ,*Bulletin of Materials Science*, **6**, 1063-1067.

Srivastava M., Ojha A.K., Chaubey S., Materny A., (2009), Synthesis and optical characterization of nanocrystalline $NiFe_2O_4$ structures, *Journal of Alloys* and *Compounds*, **481**, 515-519.

Tamjidi S., Esmaeili H., Moghadas B.K., (2019), Application of magnetic adsorbents for removal of heavy metals from wastewater: a review study, *Materials Research Express*, **6**, 102004.

Tao X., Li K., Yan H., Yang H., Li A., (2016), Simultaneous removal of acid green 25 and mercury ions from aqueous solutions using glutamine modified chitosan magnetic composite microspheres, *Environmental Pollution*, **209**, 21-29.

Teng Y., Liu Z., Yao K., Song W., Sun Y., Wang H., Xu Y., (2019), Preparation of Attapulgite/$CoFe_2O_4$ Magnetic Composites for Efficient Adsorption of Tannic Acid from Aqueous Solution, *International Journal of Environmental Research and Public Health*, **16**, 2187-2204.

Vinh N.D., Bin N., (2007), Investigation on basic blue 41 dye degradation by Fenton reaction, *VNU Journal of Science: Natural Sciences and Technology*, **23**, 275-279.

Walerczyk W., Zawadzki M., Grabowska H., (2012), Solvothermal Synthesis and Catalytic Properties of Nanocrystalline $ZnFe_{2-x}Al_xO_4$ (x=0, 1, 2) Spinels in Aniline Methylation, *Catalysis Letters*, **142**, 71-80.

Wu D., Zheng P., Chang P.R., Ma X., (2011), Preparation and characterization of magnetic rectorite/iron oxide nanocomposites and its application for the removal of the dyes, *Chemical Engineering Journal*, **174**, 489-494.

Yu H., Wang T., Dai W., Yu L., Ma N., (2018), Competitive Adsorption of Dye Species onto Biomass Nanoporous Carbon in Single and Bicomponent Systems, *Brazilian Journal* of *Chemical Engineering*, **35**, 253-264.

Zhou C.H., Keeling J., (2013), Fundamental and applied research on clay minerals: from climate and environment to nanotechnology, *Applied Clay Science*, **74**, 3-9.